

# Robust, Efficient and Low Profile Fractal Enabled EBG Incorporated Wearable Antenna for WLAN Standards

Mallavarapu Sandhya\* and Lokam Anjaneyulu

Department of Electronics and Communications Engineering, National Institute of Technology Warangal, Telangana - 506004, India

\*Email: sandhyamallavarapu@student.nitw.ac.in

## ABSTRACT

A compact, robust Koch fractal combined triangular monopole antenna incorporated with a Sierpinski fractal EBG unit cell array is proposed for integral solutions of wearable devices in WLAN standards. The fractal enabled EBG-Antenna has a modified triangular microstrip that acts as a radiator and a 2X2 array of Sierpinski square EBG unit cells as a reflective surface to enhance the performance also as a shield linking the antenna and human body. The proposed antenna demonstrations and impedance match bandwidth of 32 MHz, a gain of 7.86 dBi, Front to back ratio of 13 dB, Radiation Efficiency of 90.35 % at 2.45 GHz in free space. The EBG-Antenna performs well under different bending conditions and human tissue loading as verified by measurements. The specific absorption rate (SAR) is also evaluated and found within limits as per standards. The computed results accomplished the SAR of 0.302 W/Kg, 0.1423 W/Kg for 1 g, 10 g of tissue, respectively, which demonstrates about a 95 % drop associated with the antenna without EBG. Furthermore, the fractal loading makes the antenna compact; EBG introduced at the underside of the monopole antenna gives a high gain-bandwidth product and disengages the human body and the antenna, making the realized antenna a potential candidate with possible seamless incorporation of specified wearable applications in WLAN standards.

**Keywords:** Koch fractal; Sierpinski fractal; Electromagnetic band gap; Defected ground structure; Wireless local area networks; Wearable antenna

## NOMENCLATURE

EBG	Electromagnetic Band Gap
DGS	Defected ground structure
FBR	Front to back ratio
SAR	Specific absorption rate

## 1. INTRODUCTION

In the recent past, the utility for wearable devices in the ICT domain for on/off body applications, implantable applications, IoT, Wireless Body area networks has drawn greater attention. One of the essential parts of these devices is wearable/Textile antennas. The wearable antennas can find applications related to healthcare monitoring, emergency search services, military, activity tracking, space, and other intelligible terminals<sup>1-4</sup>. The wearable antenna is expected to be compact<sup>5-7</sup>, handy and comfortable in all the applications while giving good performance<sup>8</sup>. However, these antennas must work in near human body environment undergo deformations like bend, crumple, stretch, and folding that may affect the radiation characteristics of the antenna<sup>9</sup>. Simultaneously, less volume, lightweight, and robustness are the requisites of the fabric

antenna. To obey the health and safety standards of humans, the electromagnetic exposure limit in terms of SAR should be less in human tissue<sup>10-12</sup>. The same applies to different antenna deformations and assorted distances of separation from the human.

Many antenna designs have been fabricated and tested for their suitability to wearable applications in the open literature, including designing microstrip patch antennas<sup>13-14</sup>, PIFA<sup>15</sup>, a vertical monopole antenna, and fractal slots loaded monopole antenna<sup>16</sup>. However, all these antenna designs suffer from narrow bandwidth, low gain, and high FBR. New structures called UC-EBG planes were incorporated in the recent antenna designs to overcome all such difficulties. The UC-EBG planes can act as a reflective surface and protect the human body from radiation, giving high isolation and a small SAR<sup>17</sup>. However, some structures are electrically large, too thick, and have reduced performance.

In this work, a robust, low profile, EBG integrated textile antenna is intended without compromising the performance priorities. In general, EBG structures offer a unique feature of suppressing the surface waves by providing in-phase reflection at a particular operational band, which extensively enhances the functional characteristics of the antenna, such as gain and FBR. Compared to the published EBG loaded antenna designs, this work uses the bandgap feature of EBG (Both reflection phase and dispersion diagram approach) and a Uni-planar EBG

(UC-EBG) design. Avoiding the vertical vias in the modeling of EBG makes the proposed EBG comfortable for conformal wearable applications and allows ease of fabrication. The proposed antenna design contributes to enhanced gain, improved FBR, and significant SAR reduction compared to the previous works. In addition, the design safeguards the antenna from the torso and, as an aerial, reduces the dimension of mentioned antenna.

The remaining paper is structured as follows section 2 refers to the geometry and design of antenna and EBG structure; section 3 refers to the performance of EBG incorporated antenna in free space; section 4 refer to the bending performance of EBG integrated antenna; section 5 refers to Analysis of human tissue loading and SAR followed by conclusions.

## 2. DESIGN AND CONFIGURATION

### 2.1 Geometry of Antenna

A monopole antenna is proposed based on a second-order Koch fractal and loaded with meander line slits, as presented in Fig.1 (a)-(c). The initial shape of the monopole antenna is inspired by an equilateral triangle without cuts and notches and with a full ground plane is large in size, lower in gain, and narrowband. To enhance the parameters such as size and impedance bandwidth, the Koch fractal geometry is used on the boundary of the triangular-shaped monopole antenna, which is a self-similar design to increase the outer perimeter to achieve better performance with reduced size. An evolution of the proposed design is explored in a three-step process. A 39 mm length and width is fixed for the substrate to fit the development of wearable devices. Step 1 starts with the simple equilateral triangular radiator, whose dimensions are calculated from

$$a = \frac{2C}{3f_r \sqrt{\epsilon_r}} \tag{1}$$

Where  $a$  = side length,  $C$  = speed of light,  $f_r$  = resonant frequency and  $\epsilon_r$  = permittivity.

Height ( $h$ ) of the equilateral triangle is calculated from

$$h = \frac{\sqrt{3}}{2} a \tag{2}$$

Upon simulation using CST MW studio, the resonance peak is obtained at 4GHz approximately, which corresponds to the side of length 32.5mm for the initial triangular shape (Also verified from Eqn. (1)). Further, the Koch fractal is introduced along the side of the initial radiator to further reduction in the resonance frequency. The meander line slits parallel to the feed line are inserted, followed by truncating the ground plane to get the desired resonance in step 3 as in Fig. 1. All dimensions are optimized in CST MW studio 2019.

The geometry is built on the 39X39 mm<sup>2</sup> flexible vinyl polymer-based PTFE, commercially known as Rogers 5880 (permittivity 2.2, Thickness 0.508 mm). The equilateral triangular shape is chosen being it is physically small compared to other patch shapes and highly suitable for fabrication

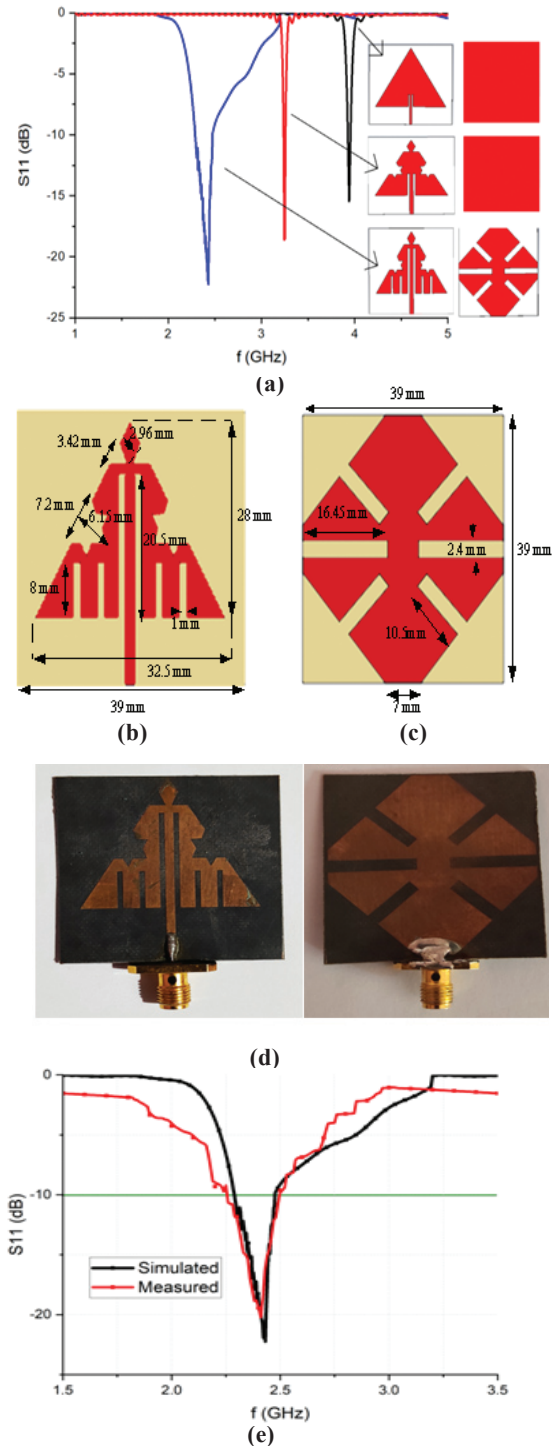


**Figure 1. (a) S11 of evolution process, (b) Front view, (c) Back view of the anticipated geometry of the monopole antenna, (d) Fabricated prototype and (e) S11 evaluation of simulated and measured antenna.**

on curved surfaces. To improve mechanical flexibility and conformability of the antenna, a meander line slits parallel to the feed line is introduced, and a compact antenna resonating at the desired frequency band of center frequency 2.45 GHz can be achieved by introducing the Koch fractal geometry. Further, a defective ground was designed to improve the impedance bandwidth. The ground plane is truncated at the corners, and rectangular slits are introduced at each truncated corner to balance the inductive attributes of the radiating element by the

capacitive load that resulted by truncating the ground plane; finally, the pure resistive input impedance is persisted. Fig. 1 (d), (e) shows the prototype and the measured and simulated reflection coefficient curves. It is observed that both are in close agreement with each other and converging to the specified bandwidth.

To get more intuition into the behavior of the anticipated antenna, it can be represented in its lumped electrical equivalent circuit. Usually, the antennas are approximated by a distributed parameter network. Therefore the lumped electrical equivalent model of monopole antenna could be imitative by the straight assumptions of microstrip elements as the combination of resistance, inductance, and capacitance. It is well known that any conducting element represents the series combination of resistance (R), and inductance (L), and a gap between the elements is represented by a parallelly connected capacitance and conductance<sup>18</sup>. Based on the cavity model of approximating the monopole antenna without slots and notches can be represented by a parallel RLC resonant circuit as revealed in Fig. 2 (a). and the elemental values can be given as<sup>19</sup>

$$R = \frac{Q}{\omega_r^2 C} \tag{3}$$

$$L = \frac{1}{\omega_r^2 C} \tag{4}$$

$$C = \frac{LW\epsilon_0\epsilon_e}{2L} \cos^2\left(\frac{\pi Y_0}{L}\right) \tag{5}$$

Where, L, W = length and width of the radiator,  $L_1$  = inductance,  $\epsilon_e$  = effective permittivity of the medium,  $\epsilon_0$  = free space permittivity,  $Y_0$  = admittance in free space,  $\omega_r$  = resonance frequency and Q = quality factor. Therefore the total input impedance of the triangular monopole patch Z is given by

$$Z = \frac{1}{\frac{1}{R} + j\omega C + \frac{1}{j\omega L}} \tag{6}$$

The proposed design used Koch fractal on the periphery and meander line slits at the base of the equilateral triangle. It involved the loading of notches at the outer boundary of the patch. After inserting the Koch fractal into the patch, the resonant frequency changes as the fractal increases the current path length. The same is confirmed by observing the current distribution of the monopole antenna represented in Fig. 5 (a). It is understood that there is a maximum current distributed in the center of the radiating element. By introducing the parallel slits and fractal-shaped notches, the current distribution is altered and thereby changing the resonant frequency. From the circuit point of view, the increment in the current path accounts for the increased inductance, which tends to decrease the resonant frequency, as presented in Fig. 2(b). Therefore the addition of series inductance and capacitance can change the circuit parameters, and new L, C are given by

$$L_{eq} = \nabla L_1 + \nabla L_2 + L \tag{7}$$

$$\frac{1}{C_{eq}} = \frac{1}{\nabla C_1} + \frac{1}{\nabla C_2} + \frac{1}{C} \tag{8}$$

Where,  $\nabla L_1, \nabla L_2, \nabla C_1,$  and  $\nabla C_2$  are additional inductance and capacitance. And the modified antenna input impedance  $Z_n$  is given by

$$Z_n = \frac{1}{\frac{1}{R_{eq}} + j\omega C_{eq} + \frac{1}{j\omega L_{eq}}} \tag{9}$$

Further, the defect in the ground structure of the proposed antenna can be represented as a simple LC parallel circuit as presented in Fig. 2(c), where the inductance represents the etched areas, and the capacitance represents the distance between the slots. The ground acts as an inductor at a frequency less than the resonance, whereas it acts as a capacitor above the resonance frequency. In other words, the defect is electrically coupled to the patch line capacitance and magnetically coupled through mutual inductance. The final electrical equivalent of the antenna estimated from ADS is shown in Fig. 2 (d). The final impedance should be obtained as

$$Z_{Total} = \frac{Z_m + Z}{Z_m Z} + Z_n + Z_L \tag{10}$$

Where,  $Z_m$  = mutual impedance,  $Z_n$  = notch loaded impedance, and  $Z_L$  = impedance of line feed

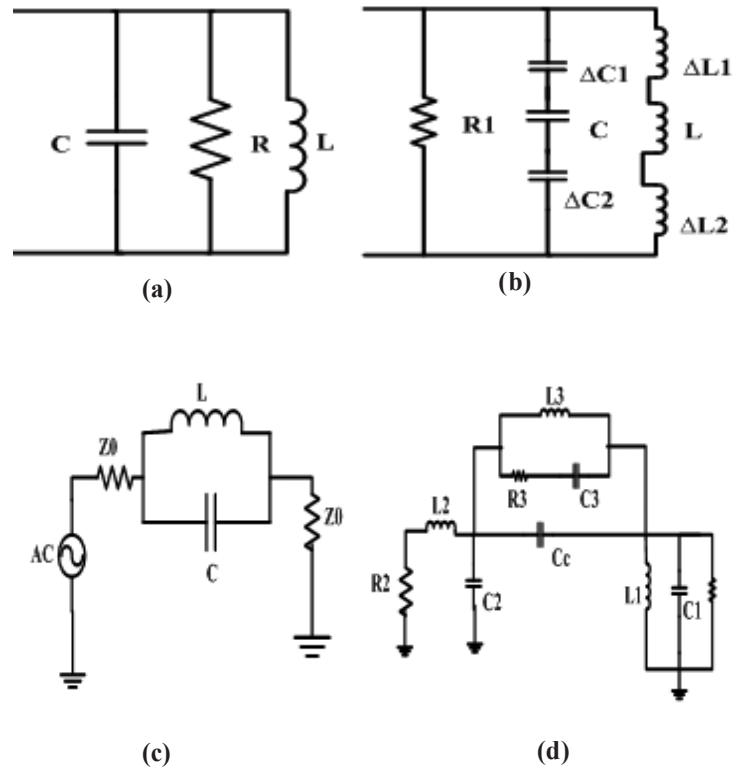


Figure 2. Equivalent circuit of: (a) Simple monopole patch (b) Notch loaded patch (c) DGS equivalent and (d) proposed antenna

**2.2 EBG Design and Electrical Equivalent**

The EBG structures are originated from conventional mushroom-like EBG. But, the existence of vias makes the fabrication process complex and might lead to inaccuracies. So vias are removed, and the via-less structure is simulated with the same dimensions as with vias. But the obtained bandgap doesn't cover the desired frequency and increases the structure's size due to a decrease in the effective inductance. Therefore, effective inductance is increased with the introduction of slots at proper separation to form a Sierpinski square fractal, as shown in Fig. 3(a). The Uni-planar EBGs are most suitable for wearable applications because of the comfortable non via structures. In the proposed design, a 35X35 mm<sup>2</sup> square unit cell is designed, in which a slot of size 1/3<sup>rd</sup> of the original square's length and width is introduced. The process is repeated for the second iteration of the fractal. This simplifies the proposed design. The unit cell is designed and optimized on the Jeans substrate as that of the antenna with a thickness of 1.57 mm.

The equivalent circuit modeled and optimized by ADS software is revealed in Fig. 3(b), where the capacitance comes from the gaps between the patch elements and space between the slots, and inductance comes from the metallic patch. The EBG surface prevents the propagation of EM waves in its bandgap region. The working of the Sierpinski square fractal EBG unit cell is elucidated by the in-phase reflection phase diagram shown in Fig. 3(c). It is accomplished that the in-phase appears at 2.45 GHz. This proves that by inserting slots, effective inductance shows increment, and volume shows decrement. On the other hand, the simulated reflection phase swings between +90 and -90 inside 1.84 to 2.67 GHz frequency. Inside this bandgap, the EBG surface offers high impedance and thereby suppressing the surface wave and leading to enhancement of the gain parameter of the antenna placed above the surface.

Figure 3(d) illustrates the dispersion diagram of the proposed EBG unit cell, where a bandgap at 2.45 GHz is

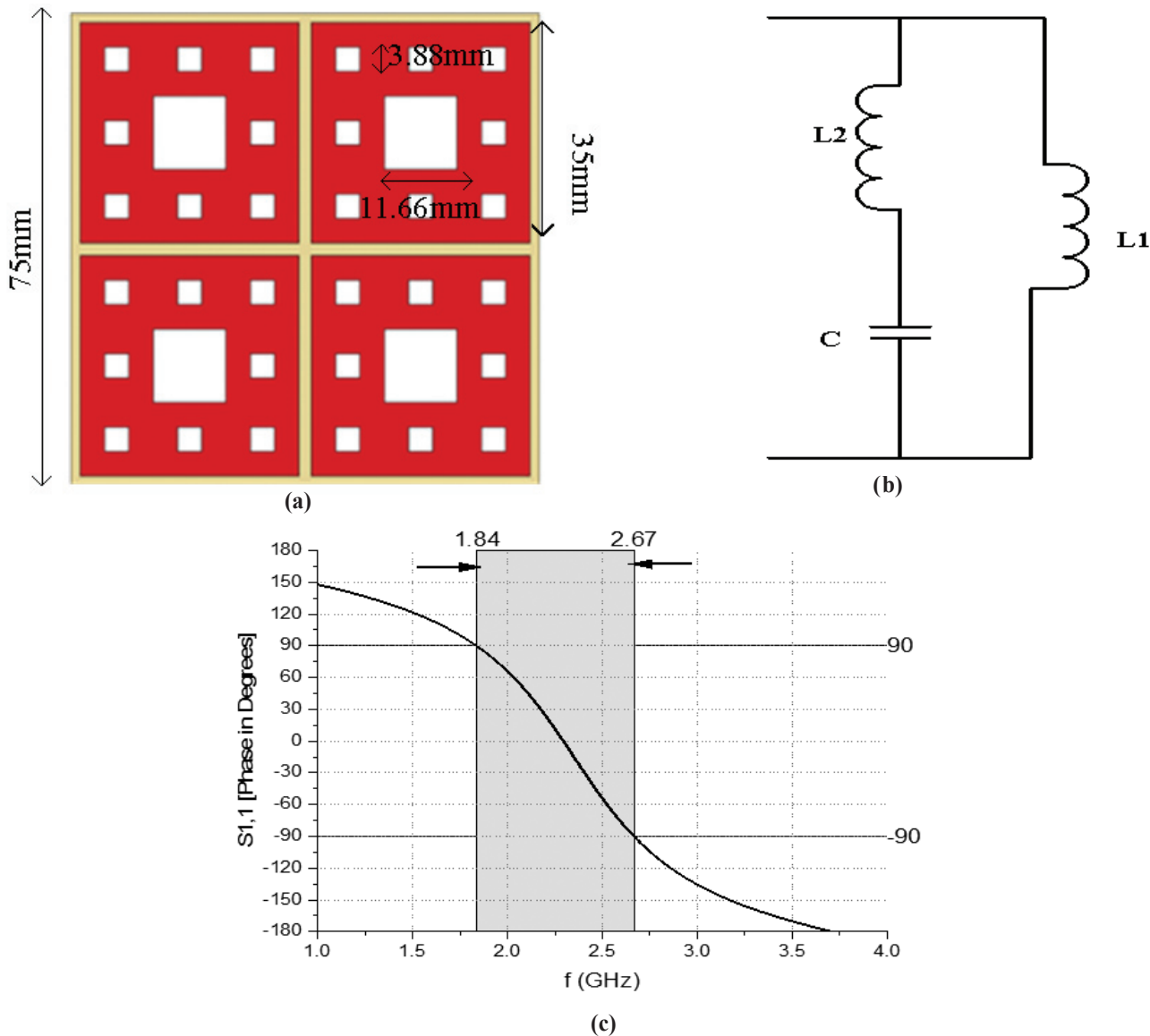


**Figure 3. (a) The layout of EBG array of unit cells (b) Equivalent circuit and (c) Reflection phase diagram.**

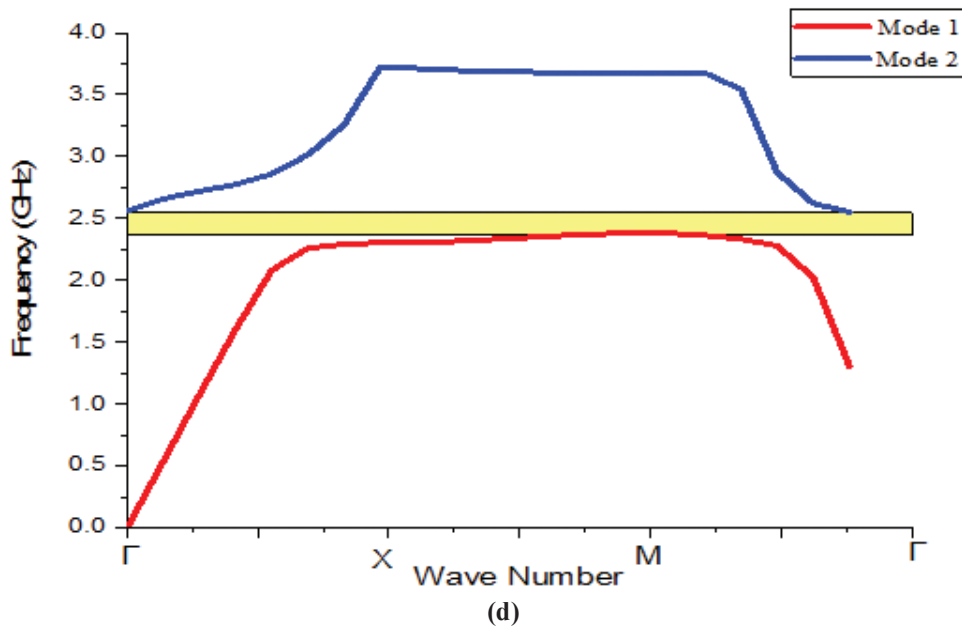


Figure 3(d). Dispersion diagram of the anticipated EBG unit cell.

exhibited. The dispersion diagram has the advantage of estimating the bandgap without calculations and measurements for the entire EBG structure. Therefore the calculation time is less. To plot the dispersion diagram, the Eigenmode solver with unit cell boundary is used in CST MW studio. The EM wave is allowed at these solutions. The dispersion diagram shows the relation between the wavenumber and the frequency for the propagating modes. There are three regions in the diagram which can have different phase shifts. In the first region  $\Gamma$ -X, the boundary phase of the x-axis varies from  $0^\circ$  to  $180^\circ$ , and the y-axis is kept at  $0^\circ$ ; in the second region, X-M, the x-axis is fixed at  $180^\circ$ , and the y-axis is varied from  $0^\circ$  to  $180^\circ$ . The region M- $\Gamma$ , both x-axis and y-axis, varies from  $0^\circ$  to  $180^\circ$ .

### 3. FREE SPACE ANALYSIS OF EBG-ANTENNA

The proposed Koch fractal-shaped monopole antenna is positioned over the EBG plane, as presented in the inset of Fig. 4 (a). A foam layer of 1 mm is positioned betwixt the

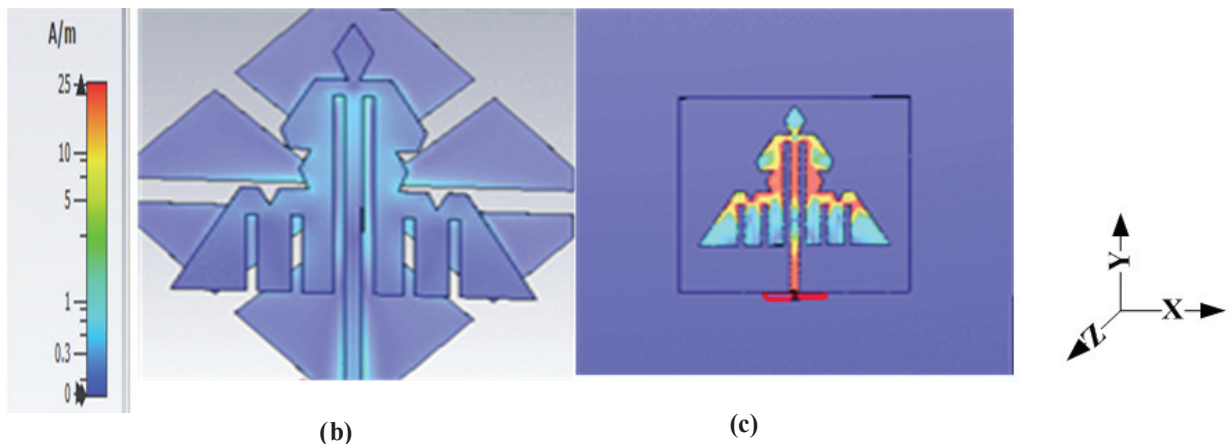
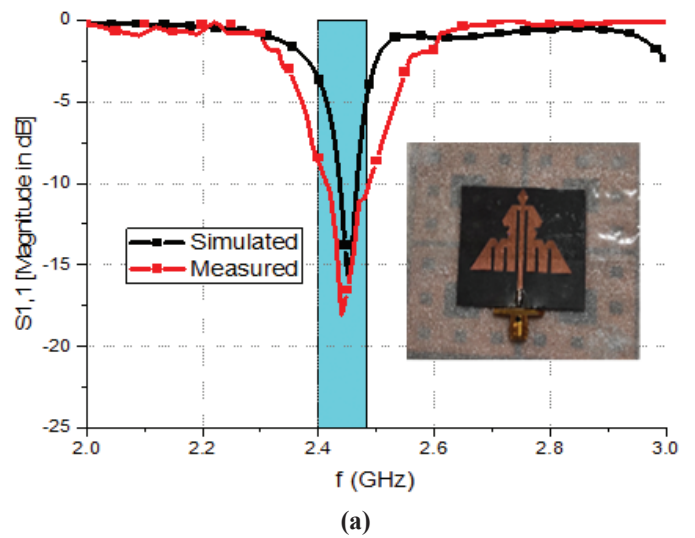


Figure 4. (a) Reflection coefficient of EBG integrated antenna (b) The current distribution of antenna alone and (c) Current distribution of EBG integrated antenna.

antenna and EBG plane to keep away from the short circuit and improve matching. Placing the antenna on the array of EBG unit cells moves the resonant frequency from the desired due to mutual coupling. Henceforth the dimensions of the antenna were altered to resonate at 2.45 GHz. Fig.4 (a) shows the reflection coefficient curve. It is seen that the EBG incorporated antenna ensures the impedance match which meets the requirement.

Further, the simulated bandwidths for antenna without EBG and with EBG are 0.35 GHz and 32 MHz, respectively is found to be in close agreement with measured bandwidths of 0.38 GHz and 48 MHz. Regardless of the shrink in bandwidth, the EBG incorporated antenna shows a better match and still covers the specified ISM band. It is because the bandwidth typically depends on the periodicity provided in between the EBG unit cells<sup>20</sup>.

Further, the integration of EBG can shrink the volume of the monopole antenna. All simulations are executed by the software CST Microwave Studio 2019 version. The surface current distribution for the antenna alone and EBG-integrated antennas at 2.45 GHz had presented in Fig. 4 (b)-(c). A significantly less surface current is observed for the antenna alone, whereas maximum current density is focused on the proposed antenna incorporated with EBG. This implies EBG also acts as a resonator and can resonate to make the antenna low profile.

Figure 5 exhibits the radiation patterns of the anticipated antenna plotted along x-z and y-z planes.

It is proved that the fractal modified antenna shows a broadside pattern and an omnidirectional pattern alongside the x-z plane and y-z plane correspondingly. However, it is always safe to consider maximum forward radiation, especially for wearable applications, which function in the juxtaposition

of the human body. This is because radiation into the body presents health risks. Therefore a directive pattern is always preferred, and the EBG integrated antenna shows maximum radiation in x-z and y-z planes. Consequently, high isolation was achieved, and it is measured in terms of FBR, which is 13 dB for the proposed antenna. Additionally, EBG incorporated antenna offers a forward gain of 7.86 dBi and an efficiency of 90.35 %.

#### 4. BENDING PERFORMANCE OF EBG INTEGRATED ANTENNA

The investigations are done for the deformation effects on the EBG incorporated antenna placed on foam cylinders of diameters 80 mm, 100 mm, and 140 mm alongside length, width directions. The diameters were carefully picked to represent the model hand, arm, and chest of the human body. Figures 6(a), (b), and (c) show the reflection coefficient variation of the antenna on various bend diameters along with length and width directions, namely on x-z and y-z planes. It is realised that there is an almost negligible effect on resonant frequency when bent. Though there is a small variation in resonant frequency, it still covers the specified ISM band frequencies.

Further, the radiation patterns for various bending situations are investigated and depicted in Fig. 7. Observing the bent scenario patterns, the proposed antenna performs well. It is acceptable with a gain variation from 7.86 dBi to 6.92 dBi, 6.05 dBi, and 5.3 dBi for bending diameters 140 mm, 100 mm, and 80 mm, respectively. Also, efficiency experiences a drop from 90.36 % to 84.85 % when deformed on 80 mm diameter. This analysis shows that the designed antenna is appropriate for conformal and wearable applications.

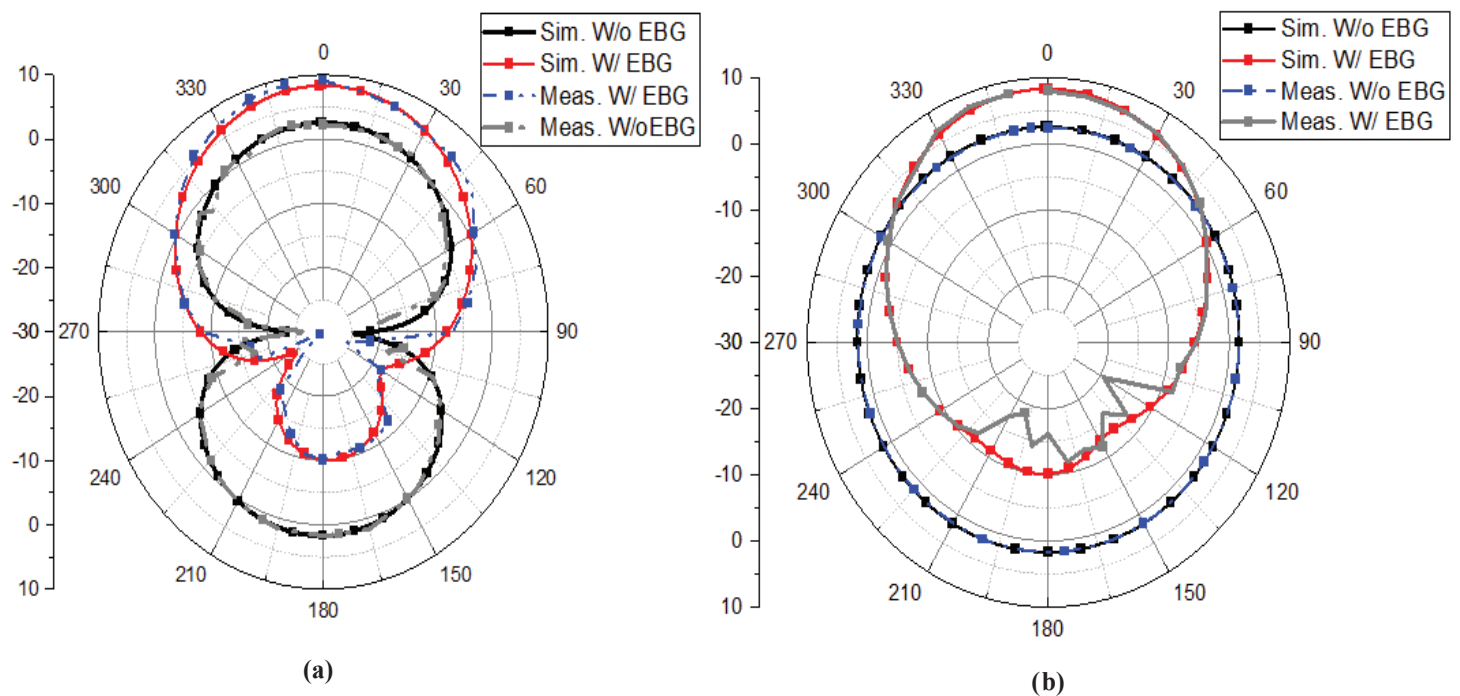


Figure 5. Radiation properties of the anticipated antenna along: (a) y-z, and (b) x-z plane at 2.45 GHz.

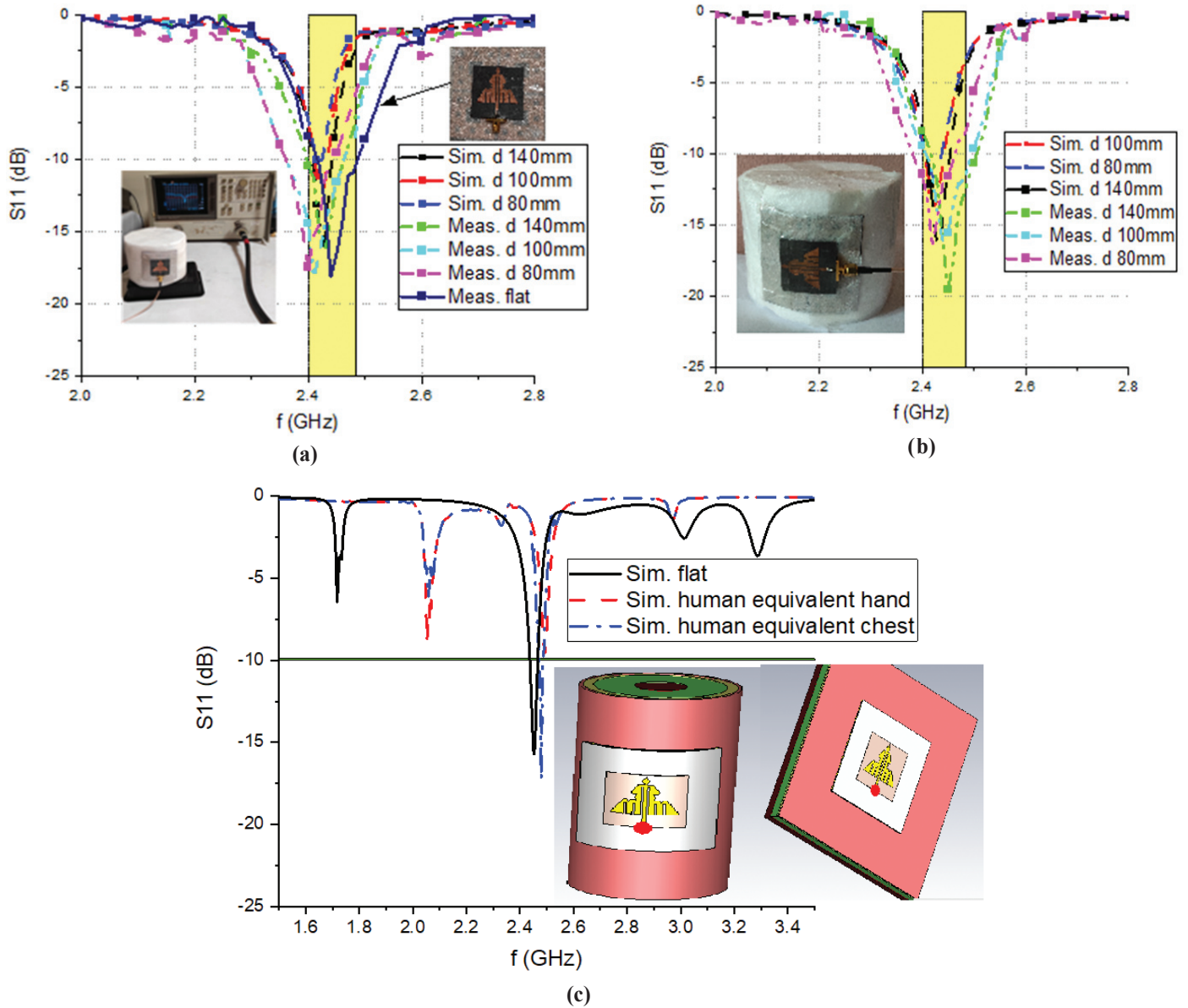


Figure 6.  $S_{11}$  variations of the anticipated antenna on various bend diameters along: (a) x-z (b) y-z planes and (c) On human equivalent hand and chest tissue.

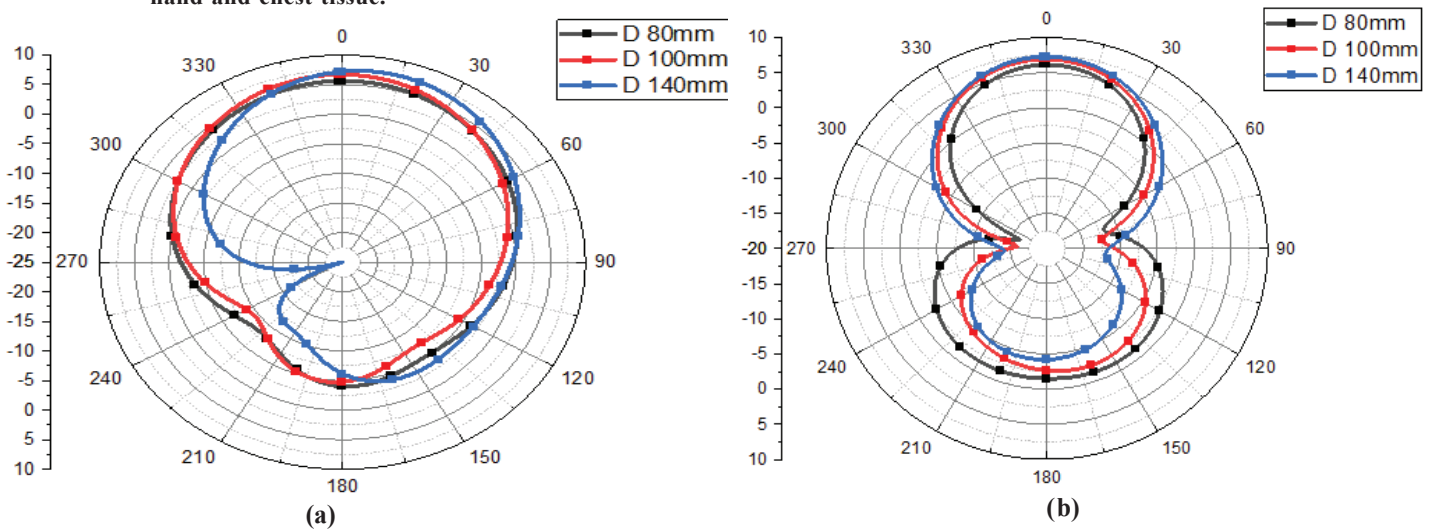


Figure 7. Radiation patterns of the anticipated antenna under various banding situations along: (a) x-z and (b) y-z planes at 2.45 GHz.

**5. ANALYSIS OF HUMAN TISSUE LOADING AND SAR**

The robustness of the anticipated model is demonstrated with the simulations and measurements performed on a real human. The simulated human tissue model takes a standard four-layer model to represent the human body. A cuboid of dimensions 150X150X40 mm<sup>3</sup> represented the chest, and the hand/ arm was represented with a cylinder of typical curvature of 80 mm, and 150 mm long. The properties such as Thickness, permittivity, density, and conductivity of the models specified are presented in Table 1<sup>21</sup>.

**Table 1. Characteristics of the human tissue model**

Property	Skin	Fat	Muscle	Bone
Thickness (mm)	2	5	20	13
Density (Kg/m <sup>3</sup> )	1001	900	1006	1008
Σ (S/m)	1.49	0.11	1.77	0.82
ε <sub>r</sub>	37.95	5.27	52.67	18.49

To verify the merits of the anticipated antenna, it is confirmed on a female whose height and weight are 151 cm and 51 Kg, respectively. The reflection coefficient performance for this scenario is plotted in Fig.8 (a) for the simulated and measured scenario. It is seen that the resonant frequencies are shifted to lower frequencies since the human body is a big lossy cylinder that acts as a sizeable dielectric layer.

The radiation properties are depicted in Fig. 8(b) for the human tissue loading of the anticipated antenna. As seen from Fig. 8(b), the radiation pattern became more directive because of the large permittivity offered by the human body than the substrate used.

The gain transfer method is used to measure the gain of the antenna since it gives simple and accurate solutions for antenna gain measurements. A known gain standard such as a Horn antenna operating from 1 GHz to 18 GHz broad frequency range is utilized to determine the gain of the antenna under test (AUT) in conjunction with the following equation:

$$G_{AUT} = \frac{P_{R2}}{P_{R3}} \cdot G_{ref} \tag{11}$$

Where, P<sub>R2</sub> = power received by the reference antenna, P<sub>R3</sub> = power received by the antenna under test, G<sub>ref</sub> = reference antenna gain, and G<sub>AUT</sub> = gain of the antenna under test.

The transmitter and the receiver antennas are separated by a distance of 1.5 m; with the transmitted power 13 dBm to 15 dBm for the measurement. Now, the gain standard is replaced with AUT (Antenna under Test), and received power is noted at each angle by rotating the AUT in the principal planes, with a transmitted power constant across all measurements. Fig.8 (c) displays the gain variation of the anticipated antenna with/without the EBG plane. The gain of EBG incorporated antenna upgraded to 7.86 dBi compared to the antenna alone and maintains the stability within the specified frequency band and is in close agreement with the measured values of gain.

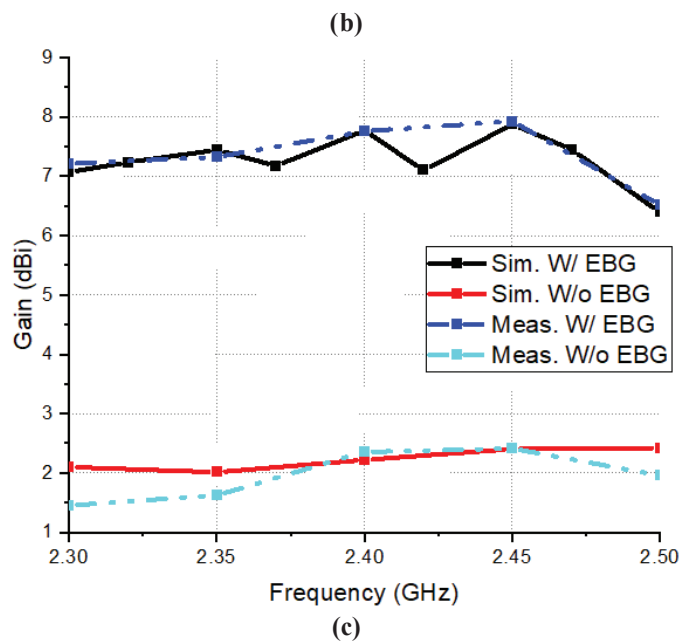
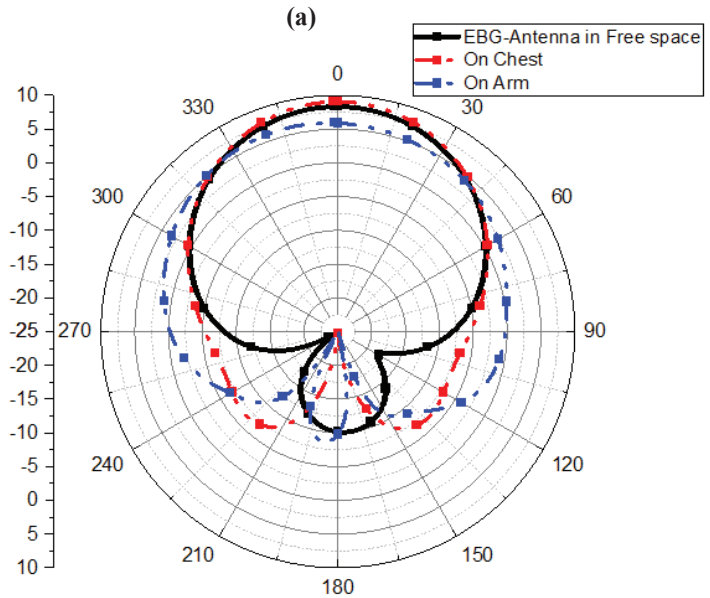
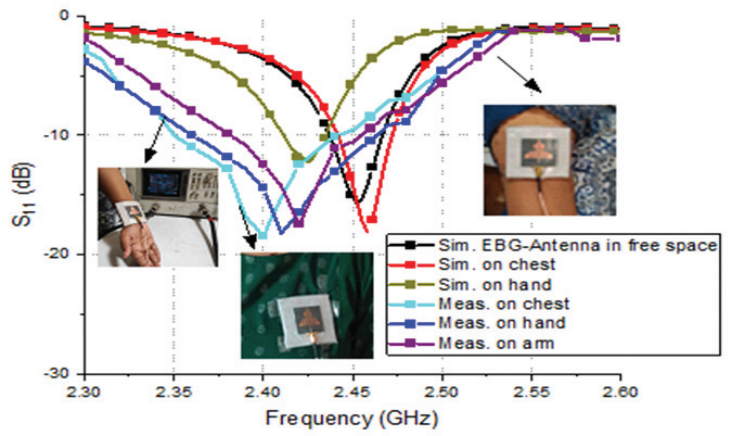


**Figure 8. (a) Variation of S11 on the human body (b) Radiation pattern at 2.45 GHz and (c) Variation of gain along with the frequency for the anticipated antenna.**

**5.1 SAR ANALYSIS**

The wearable equipment creates biological effects on the human body when worn/ operating near the human body. The exposure limit can be calculated by SAR and is given by:

$$SAR = \frac{\sigma E^2}{\rho} = \frac{J^2}{2\sigma\rho} \quad (12)$$

J= current density,  $\sigma$  (S/m) = Conductivity,  $\rho$  (Kg/m<sup>3</sup>) = Mass density of human tissue, E = intensity of electric field.

The electromagnetic exposure to the human body parts, namely the chest and arm, are evaluated for the anticipated antenna as revealed in Fig.9 and presented values in Table.2. Depending on the regulations provided by FCC (Federal Communications Commission), there is a maximum level of 1.6 W/Kg, and 2 W/Kg for a typical 1 g and 10 g of tissue individually is allowed. The four-layer phantom model specified in section IV was used to simulate the required SAR for the current scenario. Positioning the antenna at an interspace of 0 mm (On the skin), 2 mm, 4 mm, and 6 mm, respectively, from the phantom and observed the SAR values.

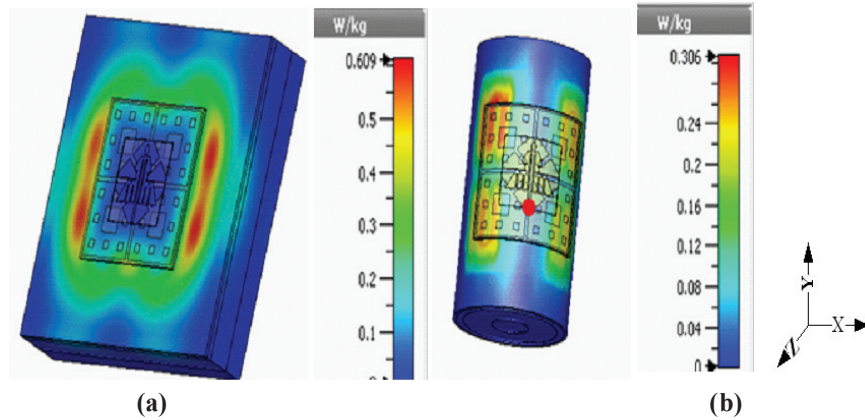


Figure 9. Evaluation of SAR for 10 g of tissue on: (a) Chest and (b) Arm.

Table 2. SAR evaluation for chest and arm models

Distance from phantom (mm)	On Chest		On Arm bent-X-axis		On Arm bent-Y-axis	
	1g	10g	1g	10g	1g	10g
0	1.291	0.608	1.499	0.305	1.506	0.305
2	1.290	0.608	0.044	0.021	0.545	0.256
4	0.302	0.142	0.405	0.198	0.406	0.199
6	0.041	0.027	0.360	0.170	0.044	0.021

Table 3. Assessment of the anticipated antenna against the previously published literature

Ref	No. of unit cells	Overall size (mm <sup>2</sup> )	Overall Thickness (mm)	Gain (dBi)	Radiation efficiency (%)	FBR (dBi)	SAR (W/Kg) /Distance from body		Frequency (GHz)
							1 g	10 g	
22	3X3	150X150	3.14	NA	NA	15	NA	0.016/1	2.45
23	3X3	120X120	4.4	6.4	NA	10	0.48/1	0.31/1	2.45
24	4X4	100X100	4.68	2.4	>40	12	NA	0.0464/1	2.45
25	1X3	30X90	8.14	4.45	NA	NA	NA	0.833/3	2.4
26	3X3	60X60	10.5	6.69	>70	NA	0.612/1	0.330/1	2.45
27	3X2	75X50	6	8.2	44	NA	0.86/1	0.414/1	2.45
28	2X1	68X38	1.57	6.3	70	NA	NA	NA	2.45
29	2X2	83X83	1.57	7.8	78.4	NA	0.64/1	0.359/1	2.38
30	3x3	65.7x65.7	4.84	3.7	NA	8	0.683/1	NA	2.45
31	3x3	55x43	7.07	8	>80	17.33	NA	NA	5.8
32	4x4	86x86	4.76	6.8	83.5	NA	0.068/1	0.022/1	3.5
33	3x3	89x83	4.18	6.2	NA	NA	0.29/1	NA	2.4
34	4x4	130.8x130.8	10.15	5.03	NA	24.5	0.0433/5	NA	2.45
Proposed	2X2	75X75	1.57	7.86	90.35	13	0.302/1	0.1423/1	2.45

From Table 2, it is seen that the values of SAR for antenna alone experience a decrement when the increased the distance between the antenna and phantom but still exceeds the standard limit. However, the SAR value for antenna integrated with EBG shows a significant drop even when directly placed on the phantom.

Wearable antennas incorporated with EBG planes at 2.45 GHz have been stated in the literature. Table.3 summarizes the designs in terms of overall size, no of unit cells in EBG array, antenna bandwidth, improved gain, and FBR and electromagnetic exposure limit. Despite the advantages, they suffer from large size and thickness, as evident from Table 3.

## 6. CONCLUSIONS

The proposed compact, high efficiency, and robust antenna incorporated with EBG is designed and tested successfully. The proposed EBG acts as a shield that can disengage the antenna from the human body, decreasing the size of the antenna. The electrical equivalent circuit is also obtained for investigating the matching potentials. The proposed EBG integrated antenna is inspected and tested for several bending and human tissue loading. The proposed antenna shows an impedance match bandwidth of 32 MHz, a gain of 7.86 dBi, Front to back ratio of 13 dB, Radiation Efficiency of 90.36 % at 2.45 GHz in free space. The measured performance is in close agreement with the simulated and far better than reported in previous works. Additionally, the SAR also analyzed and seen values very much less and in standards. This will reveal the usage of the proposed antenna for wearable prototypes and prove it to be a potential candidate for wearable applications.

## REFERENCES

1. Corchia, L.; Monti, G.; De Benedetto, E. & Tarricone, L. Wearable antennas for remote health care monitoring systems. *Int. J. Antennas Propag.*, 2017. **2017**(6), 1-11. doi: 10.1155/2017/3012341
2. Lee, H.; Tak, J. & Choi, J. Wearable Antenna Integrated into Military Berets for Indoor/Outdoor Positioning System. *IEEE Antennas Wirel. Propag. Lett.*, 2017, **16**, 1919–1922. doi: 10.1109/LAWP.2017.2688400
3. Ali, S.M.; Sovuthy, C.; Imran, M.A.; Socheatra, S.; Abbasi, Q.H. & Abidin, Z.Z. Recent advances of wearable antennas in materials, fabrication methods, designs, and their applications: State-of-the-art. *Micromachines*, 2020, **11**(10), 888. doi: 10.3390/mi11100888
4. Chen, W.L.; Wang, G.M. & Zhang, C.X. Bandwidth enhancement of a microstrip-line-fed printed wide-slot antenna with a fractal-shaped slot. *IEEE Trans. Antennas Propag.*, 2009, **57**(7), 2176–2179. doi: 10.1109/TAP.2009.2021974
5. Chen, S.J.; Kaufmann, T.; Shepherd, R.; Chivers, B.; Weng, B.; Vassallo, A. & umeaux, C. A compact, highly efficient and flexible polymer ultra-wideband antenna. *IEEE Antennas Wirel. Propag. Lett.*, 2015, **14**, 1207–1210. doi: 10.1109/LAWP.2015.2398424
6. Akhtar, F.; Naqvi, S.I.; Arshad, F.; Amin, Y. & Tenhunen, H. A flexible and compact semicircular antenna for multiple wireless communication applications. *Radioeng.*, 2018, **27**(3), 671–678. doi: 10.13164/re.2018.0671
7. Jose, J.V.; Shobha Rekh, A. & Jose, M.J. Demonstrating antenna miniaturisation for radiolocation applications using double elliptical patches. *Def. Sci. J.*, 2021, **71**(4), 515–523. doi: 10.14429/DSJ.71.16276
8. Atrash, M.E.; Abdalgalil, O.F.; Mahmoud, I.S.; Abdalla, M.A. & Zahran, S.R. Wearable high gain low SAR antenna loaded with backed all-textile EBG for WBAN applications. *IET Microwaves, Antennas Propag.*, 2020, **14**(8), 791–799. doi: 10.1049/iet-map.2019.1089
9. Ashyap, A.Y.I.; Zainal Abidin, Z.; Dahlan, S.H.; Majid, H.A.; Kamarudin, M.R.; Alomainy, A. & Noras, J.M. Highly efficient wearable CPW antenna enabled by EBG-FSS structure for medical body area network applications. *IEEE Access*, 2018, **6**, 77529–77541. doi: 10.1109/ACCESS.2018.2883379
10. Tetik, E. & D. Tetik, G. The effect of a metamaterial based wearable monopole antenna on the human body. *Celal Bayar Üniversitesi Fen Bilim. Derg.*, 2018, **14**(1), 93–97. doi: 10.18466/cbayarfbe.369051
11. Nella, A. & Gandhi, A. Lumped equivalent models of narrowband antennas and isolation enhancement in a three antennas system. *Radioeng.*, 2018, **27**(3), 646–653. doi: 10.13164/re.2018.0646
12. Gao, G.; Zhang, R.; Yang, C.; Meng, H.; Geng, W. & Hu, B. Microstrip monopole antenna with a novel UC-EBG for 2.4 GHz WBAN applications. In *IET Microwaves, Antennas Propag.*, 2019, **13**, 2319–2323. doi: 10.1049/iet-map.2019.0271
13. Hussain, S.; Hafeez, S.; Memon, S.A. & Pirzada, N. Design of Wearable Patch antenna for wireless body area networks. *Int. J. Adv. Comput. Sci. Appl.*, 2018, **9**(9), 146–151. doi: 10.14569/ijacsa.2018.090920
14. Singh, R.; Narang, N.; Singh, D. & Gupta, M. Compact wideband microstrip patch antenna design for breast cancer detection. *Def. Sci. J.*, 2021, **71**(3), 352–358. doi: 10.14429/DSJ.71.16704
15. Bai, Q. & Langley, R. Textile PIFA antenna bending. In *LAPC 2011 - 2011 Loughbrgh. Antennas Propag. Conf.*, 2011. pp.1-4. doi: 10.1109/LAPC.2011.6114061
16. Arif, A.; Zubair, M.; Ali, M.; Khan, M.U. & Mehmood, M. Q. A compact, low-profile fractal antenna for wearable on-body WBAN applications. *IEEE Antennas Wirel. Propag. Lett.*, 2019, **18**(5), 981–985. doi: 10.1109/LAWP.2019.2906829
17. Ali, U.; Ullah, S.; Khan, J.; Shafi, M.; Kamal, B.; Basir, A. & Seager, R.D. Design and SAR analysis of wearable antenna on various parts of human body, using conventional and artificial ground planes. *J. Electr. Eng.*

- Technol.*, 2017, **12**(1), 317–328.  
doi: 10.5370/JEET.2017.12.1.317
18. Siddiqui, M.G.; Saroj, A.K.; Tiwari, D. & Sayeed, S.S. Koch–Sierpinski Fractal Microstrip antenna for C/X/Ku-band applications. *Aust. J. Electr. Electron. Eng.*, 2019, **16**(4), 369–377.  
doi: 10.1080/1448837X.2019.1677121
  19. Moradikordalivand, A.; Rahman, T.A.; Ebrahimi, S. & Hakimi, S. An equivalent circuit model for broadband modified rectangular microstrip-fed monopole antenna. *Wirel. Pers. Commun.*, 2014, **77**(2), 1363–1375.  
doi: 10.1007/s11277-013-1585-y
  20. Goussetis, G.; Feresidis, A.P. & Vardaxoglou, J.C. Tailoring the AMC and EBG characteristics of periodic metallic arrays printed on grounded dielectric substrate. *IEEE Trans. Antennas Propag.*, 2006, **54**(1), 82–89.  
doi: 10.1109/TAP.2005.861575
  21. Jiang, Z.H.; Brocker, D.E.; Sieber, P.E. & Werner, D.H. A compact, low-profile metasurface-enabled antenna for wearable medical body-area network devices. *IEEE Trans. Antennas Propag.*, 2014, **62**(8), 4021–4030.  
doi: 10.1109/TAP.2014.2327650
  22. Velan, S.; Sundarsingh, E.F.; Kanagasabai, M.; Sarma, A.K.; Raviteja, C.; Sivasamy, R. & Pakkathillam, J.K. Dual-band EBG integrated monopole antenna deploying fractal geometry for wearable applications. *IEEE Antennas Wirel. Propag. Lett.*, 2015, **14**, 249–252.  
doi: 10.1109/LAWP.2014.2360710
  23. Langley, Richard. & Shaozhen, Zhu. Dual-Band Wearable Textile Antenna on an EBG Substrate. *IEEE Trans. Antennas Propag.*, 2009, **57**(4), 926–935.  
doi: 10.1109/TAP.2009.2014527
  24. Yan, S.; Soh, P.J. & Vandenbosch, G.A.E. Low-profile dual-band textile antenna with artificial magnetic conductor plane. *IEEE Trans. Antennas Propag.*, 2014, **62**(12), 6487–6490.  
doi: 10.1109/TAP.2014.2359194
  25. Afridi, A.; Ullah, S.; Khan, S.; Ahmed, A.; Khalil, A.H. & Tarar, M.A. Design of dual band wearable antenna using metamaterials. *J. Microw. Power Electromagn. Energy*, 2013, **47**(2), 126–137.  
doi: 10.1080/08327823.2013.11689852
  26. Gao, G.; Wang, S.; Zhang, R.; Yang, C. & Hu, B. Flexible EBG-backed PIFA based on conductive textile and PDMS for wearable applications. *Microw. Opt. Technol. Lett.*, 2020, **62**(4), 1733–1741.  
doi: 10.1002/mop.32224
  27. Mersani, A.; Osman, L. & Ribero, J.M. Performance of dual-band AMC antenna for wireless local area network applications. *IET Microwaves, Antennas Propag.*, 2018, **12**(6), 872–878.  
doi: 10.1049/iet-map.2017.0476
  28. Antoniadou, M.A.; Abbasi, M.A.B.; Nikolic, M.; Vryonides, P. & Nikolaou, S. Conformal wearable monopole antenna backed by a compact EBG structure for body area networks. In *2017 11th Eur. Conf. Antennas Propagation, EUCAP 2017*, 2017. pp. 164–166.  
doi: 10.23919/EuCAP.2017.7928804
  29. Arif, A.; Akram, M.R.; Riaz, K.; Zubair, M. & Mehmood, M. Q. Koch Fractal Based Wearable Antenna Backed with EBG Plane. In *17th Int. Bhurban Conf. Appl. Sci. Technol. IBCAST 2020*. pp. 642–646.  
doi: 10.1109/IBCAST47879.2020.9044575
  30. Raad, H.R.; Abbosh, A.I.; Al-Rizzo, H.M. & Rucker, D.G. Flexible and compact AMC based antenna for telemedicine applications. *IEEE Trans. Antennas Propag.*, 2013, **61**(2), 524–531.  
doi: 10.1109/TAP.2012.2223449
  31. Bahaa Qas Elias, B.; Jack Soh, P.; Abdullah Al-Hadi, A.; Hodgkinson, C. & Podilchak, S.K. Design of a compact textile crown antenna integrated with AMC for wearable IoT applications. In *15th Eur. Conf. Antennas Propagation, EuCAP 2021*. Pp.1-4  
doi: 10.23919/EuCAP51087.2021.9411413
  32. El Atrash, M.; Abdalla, M.A. & Elhennawy, H.M.A. Wearable dual-band low profile high gain low SAR antenna AMC-backed for WBAN applications. *IEEE Trans. Antennas Propag.*, 2019, **67**(10), 6378–6388.  
doi: 10.1109/TAP.2019.2923058
  33. Saeed, S.M.; Balanis, C.A.; Birtcher, C.R., Durgun, A.C. & Shaman, H.N. Wearable flexible reconfigurable antenna integrated with artificial magnetic conductor. *IEEE Antennas Wirel. Propag. Lett.*, 2017, **16**, 2396–2399.  
doi: 10.1109/LAWP.2017.2720558
  34. Paracha, K.N.; Rahim, S.K.A.; Soh, P.J.; Kamarudin, M.R.; Tan, K.G.; Lo, Y.C. & Islam, M.T. A low profile, dual-band, dual polarized antenna for indoor/outdoor wearable application. *IEEE Access*, 2019, **7**, 33277–33288.  
doi: 10.1109/ACCESS.2019.2894330

## CONTRIBUTORS

**Ms Mallavarapu Sandhya** is currently pursuing her PhD in Electronics and Communications Engineering at the National Institute of Technology Warangal. She received her M. Tech degree in Communications and Signal Processing from R.V.R & J.C. Guntur, Andhra Pradesh in 2013 and BTech degree in Electronics and communications engineering from Vignan’s Engineering College, Guntur, Andhra Pradesh, India in 2010. Her area of research is ‘Flexible and wearable multi-band antennas’. Her particular research interest is developing the conformal and radiation safe wearable antennas for WBAN applications. Her further research interests include Electromagnetic bandgap structures and defected ground structures loaded monopole antennas. Contribution in the current study: She has carried out the modelling of wearable antenna in CST tool, developed the simulation model, generated the result, managed the fabrication and testing of antenna, analysed the results and wrote the manuscript.

**Prof. Lokam Anjaneyulu** was born in 1967 in India. He received his BTech (ECE) in 1989, M. Tech in 1991, and PhD in 2010 from NIT, Warangal, and Telangana, India. He worked as a project officer at the Institute of Armament Technology, Pune, India, for five years from 1991 and was involved in the design of surface borne and air borne radar systems for clutter measurement applications. Later, he worked as a Staff Scientist at Helios Systems, Madras, India, for two years and developed Radio Wave Propagation Assessment Software Modules for Ship-borne Radars. He has been with the Department of

Electronics and communications engineering at the National Institute of Technology, Warangal, India, since 1997. His area of interest include: Computer networks, electromagnetic field theory, microwave, and radar engineering, microwave remote sensing, and neural networks & fuzzy logic systems. He has completed few defence-related R&D projects and has 100 papers to his credit in national and international conferences and journals.

Contribution in the current study: He has supervised the research work described in the paper by providing overall guidance, verifying the results, assisting to analyse the results and suggesting the organisation of the paper.